

Automatic Classification of Neuromuscular Diseases in Children Using Photoacoustic Imaging

Maja Schlereth^{1,2}, Daniel Stromer², Katharina Breininger¹, Alexandra Wagner³,
Lina Tan³, Andreas Maier², Ferdinand Knieling³

¹Department of Artificial Intelligence in Biomedical Engineering,
FAU Erlangen-Nürnberg, Erlangen

²Pattern Recognition Lab, FAU Erlangen-Nürnberg, Erlangen

³Department of Pediatrics and Adolescent Medicine, Universitätsklinik Erlangen, FAU
Erlangen-Nürnberg, Erlangen
maja.schlereth@fau.de

Abstract. Neuromuscular diseases (NMDs) cause a significant burden for both healthcare systems and society. They can lead to severe progressive muscle weakness, muscle degeneration, contracture, deformity and progressive disability. The NMDs evaluated in this study often manifest in early childhood. As subtypes of disease, e.g. Duchenne Muscular Dystrophy (DMD) and Spinal Muscular Atrophy (SMA), are difficult to differentiate at the beginning and worsen quickly, fast and reliable differential diagnosis is crucial. Photoacoustic and ultrasound imaging has shown great potential to visualize and quantify the extent of different diseases. The addition of automatic classification of such image data could further improve standard diagnostic procedures. We compare deep learning-based 2-class and 3-class classifiers based on VGG16 for differentiating healthy from diseased muscular tissue. This work shows promising results with high accuracies above 0.86 for the 3-class problem and can be used as a proof of concept for future approaches for earlier diagnosis and therapeutic monitoring of NMDs.

1 Introduction

Duchenne Muscular Dystrophy (DMD) and Spinal Muscular Atrophy (SMA) often manifest in early childhood and are hard to differentiate in early stages [1]. In severe cases, the muscles degenerate quickly, and reliable and fast diagnosis is necessary to start with the correct treatment as early as possible. Currently, confirmation of the diagnosis is typically done by genetic testing which takes up to several months [2]. To support an early assessment, imaging-based diagnosis has been proposed. Photoacoustic (PA) imaging has been investigated as an imaging modality for assessing neuromuscular diseases [3]. It comes with many advantages, as it is non-invasive, has a low acquisition time and is able to differentiate tissue composition based on their PA properties. While ultrasound (US) images depict the morphology of different tissue types, PA images contain functional information. For instance, the wavelength 800 nm helps to observe highly perfused and hemoglobin or myoglobin rich tissue, such as muscular or brain tissue [4, 5]. Regensburger et al. show that PA imaging can be successfully used to detect collagen tissue as a biomarker for DMD as muscular tissue degenerates in DMD and is replaced by collagen or fatty tissue [6]. The authors found significant differences

between healthy and diseased tissue regarding signal intensity for collagen. To analyse the data, regions of interest were manually drawn and individually evaluated for each patient. To overcome these limitations, automatic image processing and classification can be used [7]. Zhang et al. propose a traditional machine learning (ML) and a deep learning (DL) method using AlexNet and GoogLeNet for classification of breast cancer for PA images with high accuracies [8], which motivates the use of DL for diagnosis of SMA and DMD.

Our main contributions are the development and evaluation of binary classifiers that differentiate between healthy volunteers and DMD or SMA patients as a proof-of-concept study as well as a three-class classifier (healthy control, DMD, SMA) for a differential diagnosis. As DMD and SMA are difficult to differentiate in early stages, an additional indicator could speed up the diagnostic process. We compare the use of US and PA images with different wavelengths and spectrally unmixed signals (SUS) as input to the network for classification. Furthermore, we analyse the performance of the classifiers across age groups/severity and identify next steps to provide clinicians with rapid diagnostic support for muscular diseases using PA imaging.

2 Materials and methods

In the following section, we will shortly describe the data sets, image preprocessing and the experimental setup for the two-class and three-class problem to differentiate between DMD, SMA and healthy volunteers.

2.1 Datasets

Image data from two studies considering both DMD and SMA were provided by the Department of Pediatrics and Adolescent Medicine at the University Hospital of Erlangen. In these studies PA raw data were generated from 10 patients with DMD, 10 patients with SMA and 20 age-matched controls using a handheld PA system (MSOT Acuity Echo, iThera Medical GmbH, Munich, Germany). In total, the dataset consists of 10 683 valid image frames per single-wavelength (WL) or per SUS. A WL or SUS is used for visualization of different tissue types. Each task was performed with four different input images, i.e., US images, two different WL images (800 nm, 920 nm) and a SUS image (Collagen). At this stage no raw data but only preprocessed data as provided by the vendor software were available, and combining different WL/SUS images did not provide a benefit within this setup.

For DMD, which usually worsens with age, the data is divided into age groups which correlate with the progress of the disease. Three patients aged 5–6, five patients aged 7–8 and two patients aged 9–10 were examined. For SMA, the data is divided by the type of SMA. Patients with type SMA 1 exhibit more obvious symptoms than patients with SMA 2 or 3. For SMA, two patients with SMA 1, four patients with SMA 2 and four patients with SMA 3 were considered. For each class, the data is split patient-wise into training, validation and test set with ratio 0.5, 0.2, 0.3 to represent each severity stage of DMD and SMA in the test set. As the selection of the input image and network architecture was highly exploratory, we opted not to use cross-validation.

2.2 Pre-processing

To obtain the required PA images, the provided raw data was processed with the vendor specific-software to obtain four images containing one WL/SUS each. Furthermore, they were resized to 224×224 px.

2.3 Experimental setup

A VGG16 network was trained for each classification task (control vs. DMD: 2-class DMD, control vs. SMA: 2-class SMA, control vs. DMD vs. SMA: 3-class) with each of the four different input image types separately. We then used the validation set to determine the best performing WL/SUS for each task for further investigation. For both the two-class and three-class classification tasks, a weighted cross entropy loss was used as loss function to counteract class imbalance. Stochastic gradient descent (SGD) with momentum was set as optimizer. VGG16 was pre-trained on the ImageNet dataset and all weights were frozen except for the last layer [9]. Here, random augmentation techniques were applied to improve the training process (random brightness, noise, saturation, rotation and left-right flipping). Finally, the data was normalized to match ImageNet statistics. For the three-class problem, Gradient-weighted Class Activation Mapping (Grad-CAM) was used to highlight regions relevant for the network predictions from VGG16 and further investigate the network prediction. The resulting images were evaluated jointly with a pediatrician (F.K.) experienced in working with US and PA images of muscular tissue.

3 Results

As discussed in the previous section, a separate neural network was trained for each input image type and each classification task. During validation, US showed the best accuracy across all tasks with 0.96 (2-class DMD), 0.83 (2-class SMA) and 0.91 (3-class). Out of the PA images, 920 nm provides the best validation accuracy for 2-class DMD (0.95) and the 3-class case (0.83), whereas the 800 nm image showed the best accuracy for 2-class SMA.

For the final evaluation on the test set, we use the VGG16 networks trained with US and best performing PA image on the validation set, i.e., the 920 nm WL for the 2-class DMD and the 3-class case, and the 800 nm WL for the 2-class SMA. Table 1 shows the final evaluation results on unseen images. All tasks show high accuracies ranging from 0.86 to 1.00 with better performance for the networks with US input, but also discriminative power from the networks with PA input.

Table 2 shows the true positive rate broken down by disease severity for all frames from the three DMD and SMA patients of the test set, respectively, using US and 920 nm input images. As expected, we mainly see errors in patients which are in an earlier stage of disease progression, i.e., DMD at age 5 and SMA type 3. While the error rates are similar for DMD across US and 920 nm, we see a considerably larger difference in errors for SMA between the input types. Table 3 shows the confusion matrix for the 3-class case using US and 920 nm images. Figure 1 shows the activated gradients for VGG16

Tab. 1. Accuracy, recall, precision, AUC and F1 score for unseen test data for both 2-class and the 3-class tasks using US and the best PA WL/SUS as input and VGG16 as network architecture.

	Input	Accuracy	Recall	Precision	AUC	F1
2-class DMD	US	0.95	0.92	0.97	0.95	0.95
	920 nm	0.90	0.82	0.96	0.90	0.90
2-class SMA	US	1.00	1.00	0.99	0.99	0.99
	800 nm	0.86	0.97	0.69	0.89	0.86
3-class DMD	US	0.94	0.87	0.98	0.94	0.92
	920 nm	0.91	0.86	0.95	0.91	0.90
3-class SMA	US	0.94	1.00	0.99	0.94	0.99
	920 nm	0.91	0.59	0.93	0.91	0.72

Tab. 2. Percentage of frames classified correctly as DMD or SMA (true positive rate, 3-class case) for three DMD and three SMA patients broken down by different disease states using US and 920 nm images as input. Left: DMD, ages 5,7 and 10. Right: SMA type 1, 2 and 3.

	DMD			SMA		
	Age 10	Age 7	Age 5	Type 1	Type 2	Type 3
US	97 %	98 %	70 %	100 %	100 %	100 %
920 nm	90 %	99 %	69 %	100 %	49 %	31 %

Tab. 3. Relative confusion matrix for US and 920 nm of the 3-class case comparing network prediction and ground truth (GT) labels. Diagonal elements shows percentage of correctly classified frames.

		Predicted					
		US		920 nm			
GT	Healthy	98.6 %	1.3 %	0.1 %	97.3 %	2.3 %	0.4 %
	DMD	12.5 %	87.5 %	0 %	14 %	86 %	0 %
	SMA	0 %	0 %	100 %	33.6 %	7.1 %	59.3 %

in layer 29 of six different 920 nm WL images. One example each for SMA, DMD and healthy control which is correctly classified and one example each which is wrongly classified is exhibited. The visualization using Grad-CAM shows activated gradients for correctly classified SMA in the central muscle area. In the wrongly classified scan, no central activation is visible. For correctly classified DMD, strong activations are visible in more superficial muscular areas. For the correctly classified healthy scan, no central activations are present.

4 Discussion

In this paper, we show initial results for the classification of neuromuscular diseases based on US and PA images for pediatric patients suffering from DMD and SMA. These initial results on a small dataset are promising across the different settings and tasks.

While US imaging provides slightly better quantitative classification results compared to PA input images in our study, clinical observations indicate the potential for an added value by PA images as it may offer finer gradation than US alone. Specifically, it is able to enrich the imaging data with functional information beyond the morphological structures visible in US. As we could not demonstrate a benefit in preliminary experiments yet, further research will have to investigate the potential of combining PA and US images and the limitations of this strategy under a more careful preprocessing scheme.

The dataset in the current study was acquired from a small study population with a comparatively simple network architecture and further evaluation has to be performed to validate our findings. In preliminary experiments, other architectures such as AlexNet, ResNet and EfficientNet-B0 were also considered and performed on par or slightly lower compared to VGG16. An evaluation of this performance difference will be interesting to

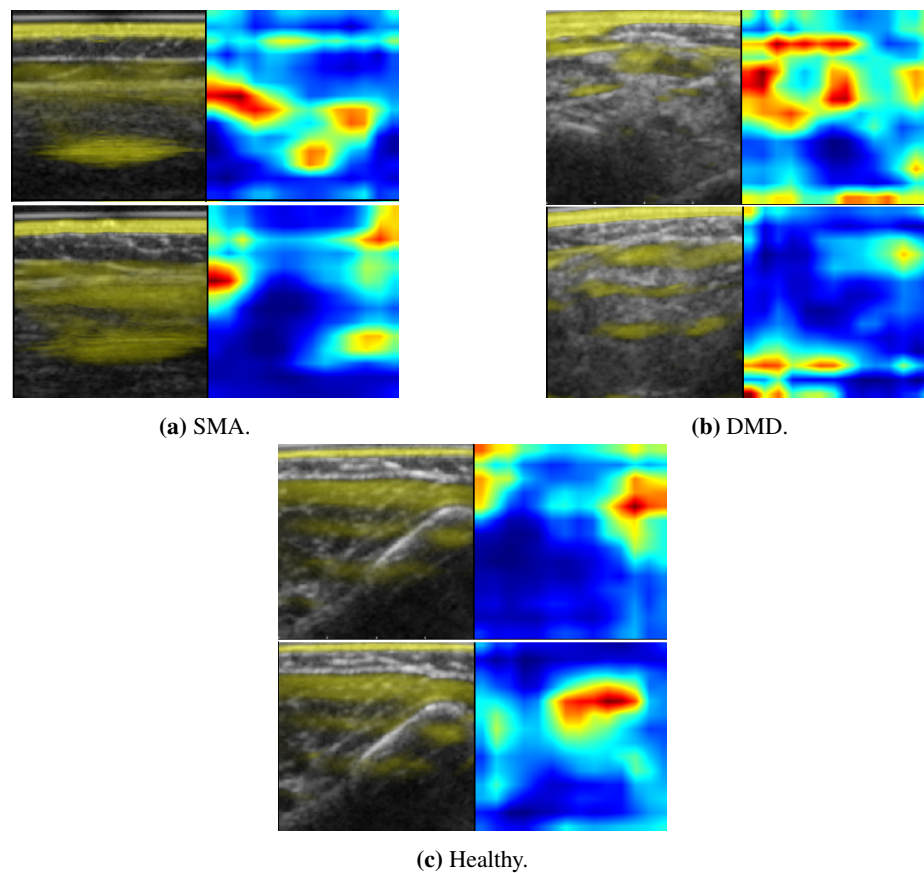


Fig. 1. Grad-CAM results for (a) SMA, (b) DMD and (c) healthy. Left: 920 nm image (yellow) overlaid on US image, right: heatmap of activated gradients. Highly activated regions are depicted in red and localize class discriminative features. Top row is correctly classified, bottom row is wrongly classified.

discuss in future work. Due to the small dataset, we opted for a frame-wise evaluation of the classification. We expect that the classification performance can be increased further if multiple frames or scans of one patient are considered, e.g., via majority voting. On a larger dataset, we further see considerable potential for using multiple input images jointly for a classification to combine complementary information across US and PA, i.e., combining morphology and functional information. This also translates to other applications such as inflammatory diseases where increased blood circulation in the injured region may be identified in the PA images whereas morphological changes can be identified in US images.

Our analysis shows a connection between the number of correctly classified scans and age for DMD, and correctly classified frames and subtype for SMA. This matches well with the fact that older patients in the case of DMD also exhibit more distinct clinical symptoms [1] and that clinical symptoms vary in severeness in the different SMA subtypes [10]. It can therefore be postulated that the disease progression also has clear impact both on the measured US and PA signal. US and PA could potentially be used to monitor treatment process and medication response to support personalized treatment planning and assessment if further research confirms predictability of severity for each disease. Despite the slightly lower performance of PA compared to US, PA's inherent properties will make it an interesting choice for future applications.

References

1. Feldman EL. Atlas of neuromuscular diseases. Springer, 2005.
2. Stuberger WA. Muscular dystrophy and spinal muscular atrophy. Physical therapy for children (2006), pp. 421–452.
3. Wagner AL, Danko V, Federle A, Klett D, Simon D, Heiss R et al. Precision of hand-held multispectral optoacoustic tomography for muscle imaging. *Photoacoustics* 21 (2021), p. 100220.
4. Phelps JE, Vishwanath K, Chang VTC, Ramanujam N. Rapid ratiometric determination of hemoglobin concentration using UV-VIS diffuse reflectance at isosbestic wavelengths. *Opt Express* 18.18 (2010), pp. 18779–18792.
5. Kirchner T, Gröhl J, Holzwarth N, Herrera MA, Hernández-Aguilera A, Santos E et al. Photoacoustic monitoring of blood oxygenation during neurosurgical interventions. *Photons Plus Ultrasound*. Ed. by Oraevsky AA, Wang LV. Vol. 10878. International Society for Optics and Photonics. SPIE, 2019, pp. 14–18.
6. Regensburger AP, Fonteyne LM, Jüngert J, Wagner AL, Gerhalter T, Nagel AM et al. Detection of collagens by multispectral optoacoustic tomography as an imaging biomarker for Duchenne muscular dystrophy. *Nat Med* 25.12 (2019), pp. 1905–1915.
7. Gröhl J, Schellenberg M, Dreher K, Maier-Hein L. Deep learning for biomedical photoacoustic imaging: A review. *Photoacoustics* 22 (2021), p. 100241.
8. Zhang J, Chen B, Zhou M, Lan H, Gao F. Photoacoustic image classification and segmentation of breast cancer: A feasibility study. *IEEE Access* 7 (2019), pp. 5457–5466.
9. Simonyan K, Zisserman A. Very deep convolutional networks for large-scale image recognition. <https://arxiv.org/pdf/1409.1556>. 2014.
10. Schara U, Schneider-Gold CJ, Schrank B. Klinik und Transition neuromuskulärer Erkrankungen. Berlin: Springer, 2015.